Inorganic Chemistry

pubs.acs.org/IC Article

Borafluorene-Mediated Sulfur Activation: Isolation of Boryl-Linked S_7 and S_8 Catenates and Related Chalcogenide Molecules

Nathan C. Frey, Kimberly K. Hollister, Peter Müller, Diane A. Dickie, Charles Edwin Webster,* and Robert J. Gilliard, Jr.*

Cite This: *Inorg. Chem.* 2024, 63, 17639−17650 Read Online

ACCESS | Metrics & More | Article Recommendations | Supporting Information

ABSTRACT: Although the activation of elemental sulfur by main group compounds is well-documented in the literature, the products of such reactions are often heterocyclic in nature. However, the isolation and characterization of sulfur catenates (i.e., acyclic sulfur chains) is significantly less common. In this study, we report the activation of elemental sulfur by the 9-CAAC-9-borafluorene radical (**1**) and anion (**2**) (CAAC = (2,6-diisopropylphenyl)-4,4-diethyl-2,2-dimethyl-pyrrolidin-5-ylidene) to form boron−sulfur catenates (**3**−**6**). From the isolation of the octasulfide-bridged compound **3**, a sulfur extrusion reaction using 1,3,4,5-tetramethylimidazol-2-ylidene (IMe_4) was used to decrease the sulfide chain length from eight to seven (**4**). Bonding analysis of compounds **3**−**6** was performed using density functional theory, which elucidated the nature of the sulfur−sulfur bonding observed within these compounds. We also report the synthesis of a series of borafluorene-chalcogenide species (**7**−**9**), via diphenyl dichalcogenide activation, which portray characteristics described by an internal heavy atom effect. Compounds **7**−**9** each exhibit blue fluorescence, with the lowest energy emissive process ($S_2 \rightarrow S_0$) at 436 nm (**7** and **8**) and 431 nm (**9**). The $S_1 \rightarrow S_0$ emission is not observed experimentally due to a Laporte forbidden transition. Density functional theory was employed to investigate the frontier molecular orbitals and absorption and emission profiles of compounds **7**−**9**.

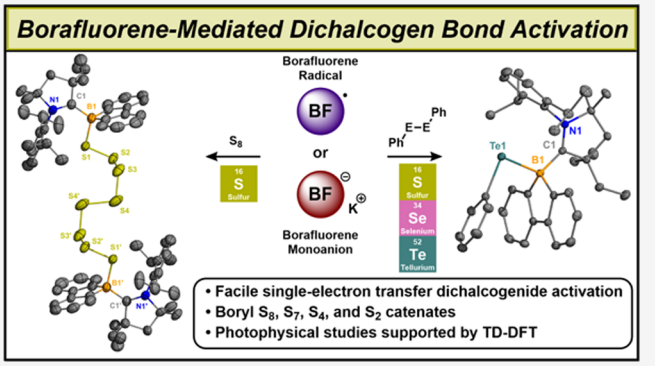

INTRODUCTION

In recent years, there has been a surge in the number of reported electron-rich boron heterocycles due to their unusual structural properties and ability to activate chemical bonds.[1−32] Boron-based radicals[20,24−31] and anions[5,10−19] have been used as chemical synthons for the preparation of compounds containing new boron-element bonds. By increasing the electron density at the boron center, the now-filled *p*-orbital allows such systems to act as nucleophiles[2−5,11−13,20,32] or single-electron transfer reagents.[15,22,23,33] These compounds have showcased abundant reactivity toward a variety of industrially relevant small molecules (e.g., H_2, CO_2, CO)[12,20,21,34] as well as the activation of chalcogens, particularly sulfur,[35−40] selenium,[23,38,40−45] and tellurium.[38,41,44,46]

In its most common allotrope, sulfur exists as S_8, or octasulfur, which is a cyclic allotrope consisting of eight disulfide (S−S) bonds.[47] Because of their prevalence in biological[48−50] and pharmaceutical applications,[51,52] as well as a promising future in the battery field via lithium sulfur batteries,[53,54] there is an ever-growing desire to activate disulfide bonds. Activation of elemental sulfur has been shown to result in heterocyclic, polysulfide-containing species. For example, one of the earliest examples of elemental sulfur activation by a transition metal was reported by Samuel in 1966, in which a titanocene pentasulfide (TiS_5) heterocycle was generated (Figure 1A).[55] Similar structural motifs have been observed in main-group element-mediated sulfur activation. Examples include the SiS_4 motif reported by Goto,[56] the BS_2, BS_4, and BS_6 heterocycles synthesized by Cui,[36] and the asymmetric B_2S_3 heterocycles described by Braunschweig (Figure 1A).[38] Despite the number of polysulfide-containing heterocycles in the literature, acyclic polysulfide chains are rare.[57] Utilizing both base-stabilized diboranes and boron-based Lewis pairs, Stephan isolated neutral and ionic boron−sulfur catenates with S_4 and S_7 chains, respectively (Figure 1B).[58,59] Fitchett activated S_8 using Bi(NONAr) radicals to form a unique Bi−S_4 dimer connected through S-based pancake bonds (Figure 1B).[60] During the final

Received: June 13, 2024
Revised: August 16, 2024
Accepted: August 22, 2024
Published: September 6, 2024

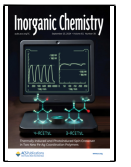

https://doi.org/10.1021/acs.inorgchem.4c02459
Inorg. Chem. 2024, 63, 17639−17650

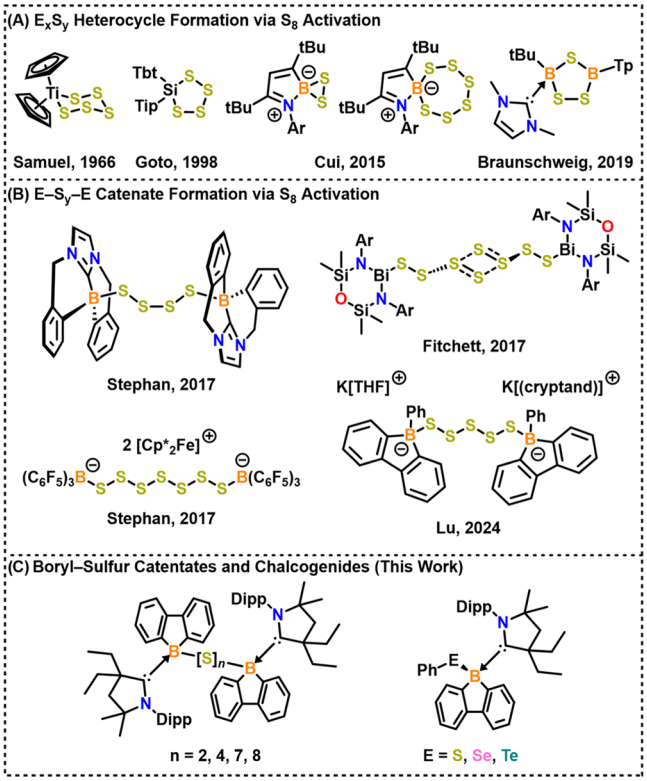

Figure 1. (A) Examples of E_xS_n (E = Ti, Si, B) heterocycles formed from S_8 activation (Tbt = 2,4,6-tris[bis(trimethylsilyl)methyl]-phenyl; Tip = 2,4,6-triisopropylphenyl; Tp = 2,6-bis(2,4,6-trimethylphenyl)-phenyl). (B) Examples of sulfur catenates formed from S_8 activation. (C) Boryl−sulfur catenates and chalcogenides (this work).

preparation of this manuscript, Lu published a dianionic version of an S_5-linked bis(borafluorene) (Figure 1B).[61] The chemistry involving the insertion of S into the B−C bonds of pentaphenyl borole,[62] as well as 9-*o*-carboranyl-substituted 9-borafluorene[63] have also been explored.

Our laboratory has recently showcased a variety of reactions with the 9-carbene-9-borafluorene anions toward main-group and transition metal halides,[10] selenium,[23] CO_2,[20] and diketones.[10,22,33] However, the reactivity of the 9-carbene-9-borafluorene radical[31] has remained relatively unexplored. This study presents reactions of the cyclic(alkyl)(amino) carbene-stabilized borafluorene radical and anion toward dichalcogenide bonds and shows rare instances of compounds containing sulfur-linked borafluorene units, some of which possess polysulfide chains that are among the longest that have been crystallographically identified (Figure 1C).

RESULTS AND DISCUSSION

The combination of 9-CAAC-9-borafluorene radical (CAAC = (2,6-diisopropylphenyl)-4,4-diethyl-2,2-dimethyl-pyrrolidin-5-ylidene) (**1**) and 0.5 equiv of elemental sulfur (S_8) in diethyl ether (Et_2O) resulted in a rapid color change from deep purple to pink. An off-white suspension formed during the course of the 2 h reaction and was collected by filtration and identified as compound **3** (64% yield) (Scheme 1). Compound **3** was characterized by ^{1}H NMR spectroscopy and showed a multiplet at 3.03 ppm, corresponding to the methine protons of the 2,6-diisopropylphenyl group. The ^{11}B{^{1}H} NMR spectrum revealed a single resonance at −4.6 ppm, which is consistent with a tetracoordinate borafluorene species.[34]

The ^{1}H NMR spectrum of the filtrate showed peaks corresponding to multiple methine environments, indicating additional sulfur-activation products formed during the reaction. Despite modifying the reaction conditions and workup procedures, the other products could not be isolated. In order to understand the side products that could be formed from this reaction, other methods of disulfide bond activation were considered. Traditionally, there are three mechanisms of disulfide bond activation: electrophilic, radical, and nucleophilic.[64] Accordingly, we pursued S_8 reactivity studies with the more electron-rich CAAC-stabilized borafluorene anion (**2**), speculating that similar sulfur-activation products may form. From these reactions (Scheme 2), compounds **4**, **5**, and **6** were identified by single-crystal X-ray diffraction studies of suitable crystals. However, based on NMR studies, all reactions yielded complex mixtures of products containing S_n chains of varying length. These products possess similar solubilities in organic solvents, which preclude their isolation on a preparative scale.

In an effort to isolate chain lengths shorter than S_8, sulfur extrusion reactions were considered. For decades, sulfur extrusion from cyclic systems has been used to mediate the formation of new bonds and promote aromaticity by coupling aryl C−C bonds.[65] These reactions typically proceed using heat or strongly donating Lewis bases such as phosphines[65−68] or N-heterocyclic carbenes.[69,70] Combining compound **3** and 1,3,4,5-tetramethylimidazol-2-ylidene (IMe_4)[71] in an equimolar ratio in toluene led to the immediate formation of a brown solution containing a white precipitate. After stirring for 2 h, the white precipitate was collected by filtration and washed with toluene to give compound **4** in 29% yield (Scheme 3). While the conversion to compound **4** is clean, the low isolated yield is due to its partial solubility in toluene, which is needed to wash away S═IMe_4. As expected, the NMR spectra of compounds **3** and **4** are similar, with comparable ^{11}B{^{1}H} resonances (−4.6 vs −5.4 ppm) and similar methine proton environments in the ^{1}H NMR spectra (3.03 ppm (**3**) vs 3.00

Scheme 1. Synthesis of Compound 3 via S_8 Activation of Borafluorene Radical[a]

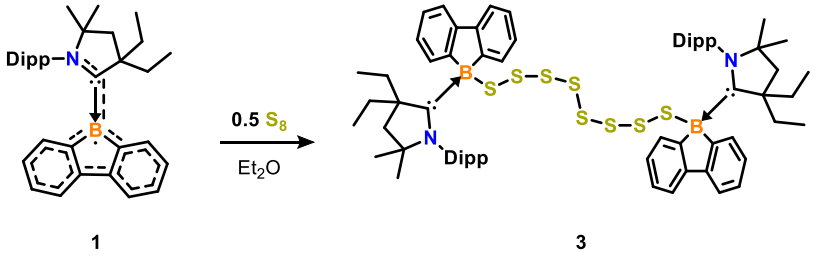

[a]Dashed lines in **1** represent delocalization of the radical across the ligand and boron heterocycle.

https://doi.org/10.1021/acs.inorgchem.4c02459
Inorg. Chem. 2024, 63, 17639−17650

Scheme 2. Compounds Identified via Single-Crystal X-ray Diffraction from Reactions between Borafluorene Anion (2) and S_8

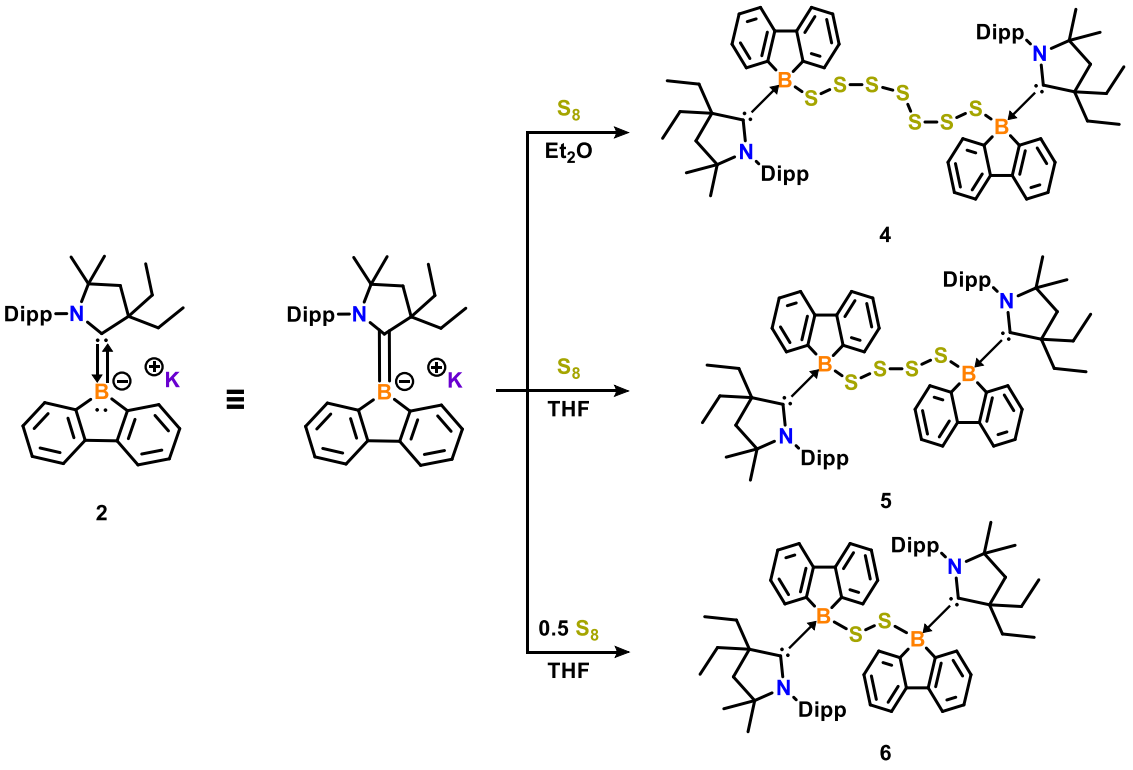

Scheme 3. 1,3,4,5-Tetramethylimidazol-2-ylidene (IMe_4)-Initiated Sulfur Extrusion from the Boryl-S_8–Boryl Complex to Form the Boryl-S_7–Boryl Compound 4

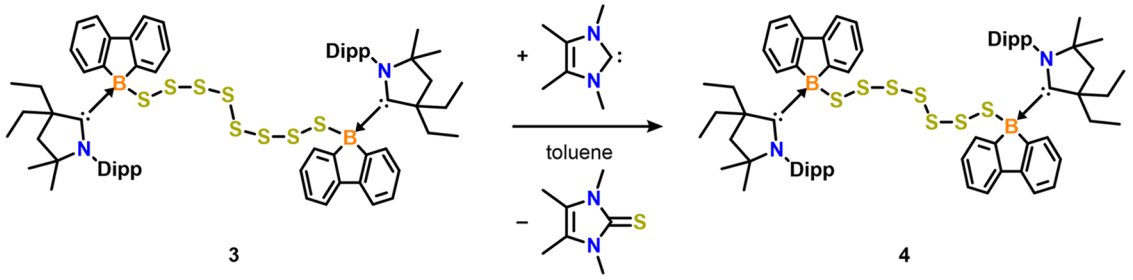

ppm (**4**)). Colorless single-crystals of **4** were grown by vapor diffusion of pentane into a THF solution of **4** and single-crystal X-ray diffraction was used to confirm product identity.

Structural characterization of compounds **3**–**6** was conducted via single-crystal X-ray diffraction studies (Figure 2). The polysulfide bridges in compounds **3** and **4** represent uncommon examples of S_n chains where $n \geq 7$.[59,72−83] Of the reported 268 polysulfide chains ($n \geq 3$) reported in the Cambridge Structural Database, only 20 structures possess sulfur chains longer than $n = 7$.[57] Among these polysulfide chains are the S_{12}^{2-} anions reported by Edelmann[76] and Wang,[77] which are the longest polysulfide chains reported to date. Although there have been several isolated species of alkyl-linked borafluorenes,[84,85] compounds **3**–**6** are unique examples of heteroatom-linked borafluorene moieties. Interestingly, the length of the B1–S1 bond (2.01(1) Å for **3**, 1.980(3) Å for **4**, 1.962(6) Å for **5**, 1.951(2) Å for **6**) is longer than the sum of covalent radii (R(B–S) = 1.89 Å),[86] which can be explained by the electron-rich character of the boron center due to donation from the CAAC ligand. The observed distances in the S–S bonds of compounds **3**–**6** are reported in Table S2. Further analysis of the electronic environment around the polysulfide chains of compounds **3**–**6** was performed by determining the dihedral angles of various points of interest within each molecule (Table S3). Most notably, the internal S3–S4–S4′–S3′ dihedral of compound **3** (180.0(3)°) and the B1–S1–S1′–B1′ dihedral of compound **6** (−180.00(8)°) are identical, whereas the dihedral angles of compounds **4** and **5** are much closer to the ideal 90°. While this geometric configuration of compound **3** can be ascribed to electron-pair repulsion from the neighboring sulfur atoms, the *anti*-configuration of compound **6** can be attributed to steric hindrance between the two carbene ligands. Despite this, the remaining dihedral angles of compounds **3** and **4** are much closer to the ideal 90°, thereby minimizing electron-pair repulsion along the polysulfide chain (Table 1).

Further investigation of the bonding of compounds **3**–**6** was performed via intrinsic bonding orbital (IBO) analysis. Tabulation of Wiberg bond indices (WBI) of B–S and S–S bonds is available in Tables S16–19. With the exception of compound **6**, each sulfur catenate has π delocalization across B1–S1–S2 as a result of slight orbital overlap between these

https://doi.org/10.1021/acs.inorgchem.4c02459
Inorg. Chem. 2024, 63, 17639−17650

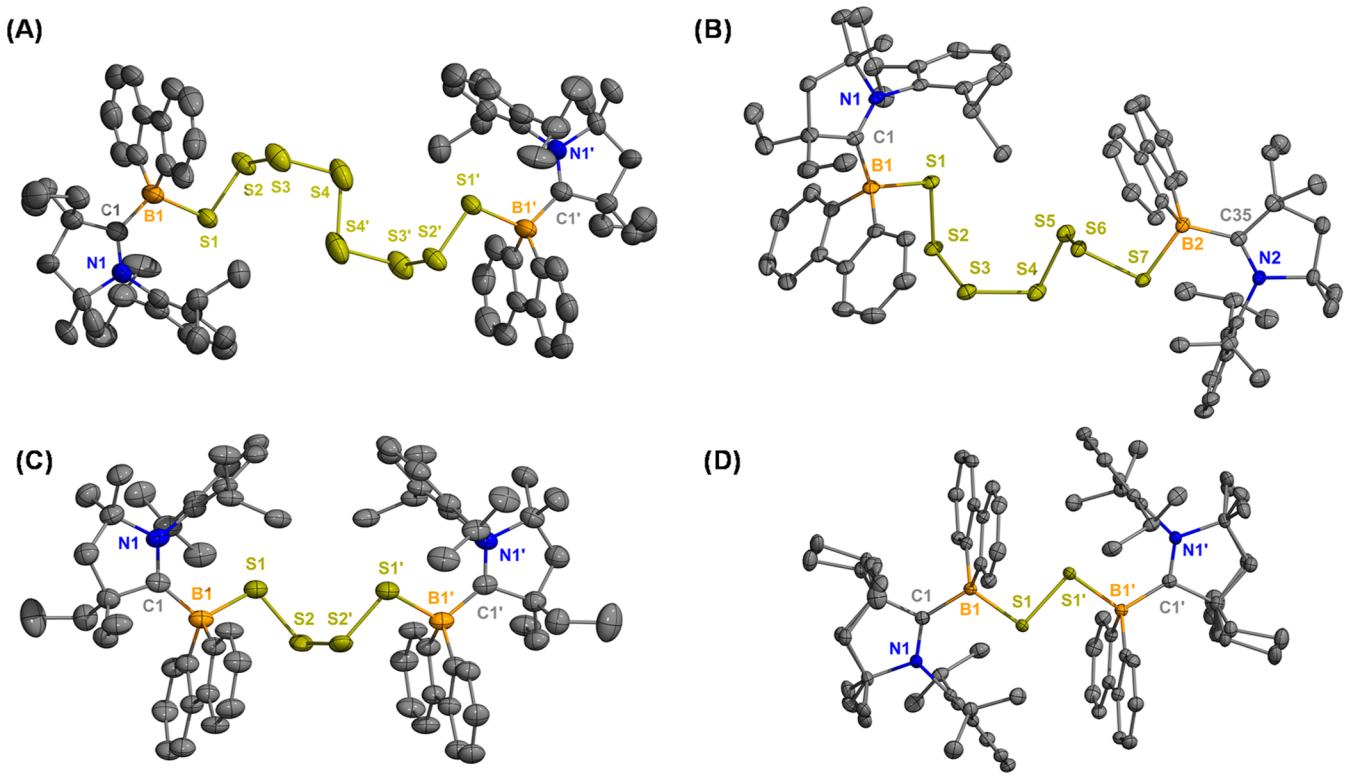

Figure 2. Molecular structures of **3** (A), **4** (B), **5** (C), and **6** (D). Thermal ellipsoids are shown at 50% probability. H atoms and solvent omitted for clarity.

Table 1. Selected Bond Distances (Å) in Compounds 3−6

compd.	B1−S1	B1−C1	C1−N1	S1−S1′/S2	S2−S2′/S3	S3−S4	S4−S4′/S5
3	2.01(1)	1.64(1)	1.30(1)	2.03(1)	2.112(6)	2.051(5)	2.267(7)
4	1.980(3)	1.656(4)	1.312(4)	2.0527(9)	2.0589(9)	2.065(1)	2.057(1)
5	1.962(6)	1.653(8)	1.301(6)	2.052(2)	2.051(2)		
6	1.951(2)	1.652(3)	1.309(2)	2.0939(6)			

three atoms. Additionally, compounds **3**−**6** also exhibit delocalized π interactions, as confirmed by WBI (Tables S16−S19) and delocalization index (Tables S20−S23) analysis.

The bonding in compound **3** was analyzed by considering the S3−S4−S4′−S3′ dihedral angle (180.3(0)°). Figure 3 shows that, although the S4 and S4′ are connected through a sigma bonding interaction, the sulfurs are oriented in a direction that maximizes overlap between the lone pairs of each sulfur center (Figure 3A). As a result, the WBI of the S4−S4′ bond was calculated to be 0.811, which shows a diminished bonding interaction between these two species, primarily due to overlapping lone pairs of each sulfur atom. The 180° dihedral angle also results in a lower degree of electron delocalization from S4 to S4′ (Table S20). The same reasoning was extended to the elongated bond distance between S2−S3/S2′−S3′. However, the orbital overlap of the p_π lone pairs between S2 and S3 is less than that of S4−S4′, which results in the S2−S3 bond distance being slightly shorter than S4−S4′ (Tables S2 and S16). The dihedral angle is closer to the ideal 90° for S1−S2/S1′−S2′, which minimizes lone pair repulsion (Figure 3B), resulting in a longer S−S distance (WBI = 1.00). In compounds **4** and **5**, however, all of the S−S bonds are more single bond in character due to decreased π overlap between sulfur atoms, as indicated by the dihedral angles about

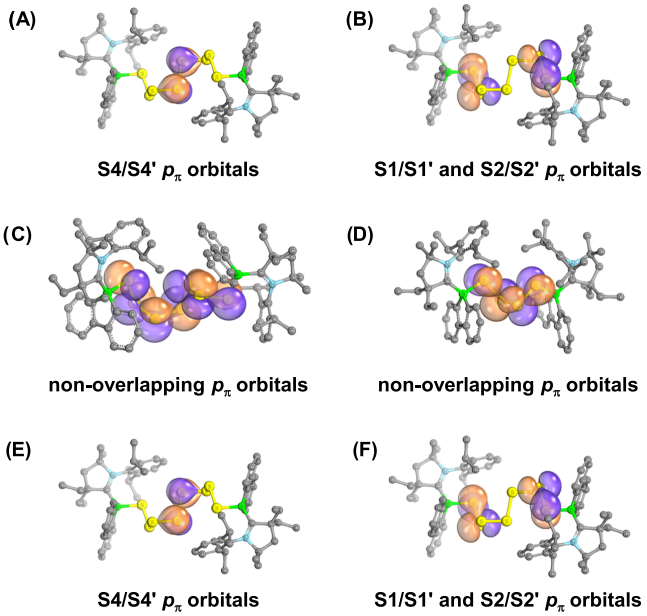

Figure 3. Intrinsic bonding orbitals (IBO) of the solid-state structure of compounds **3** (A and B), **4** (C), **5** (D), and **6** (E and F). Hydrogen atoms omitted for clarity.

https://doi.org/10.1021/acs.inorgchem.4c02459
Inorg. Chem. 2024, 63, 17639−17650

Scheme 4. Synthesis of Boryl Chalcogenides 7−9 via Borafluorene Radical- or Anion-Mediated Dichalcogenide Activation[a]

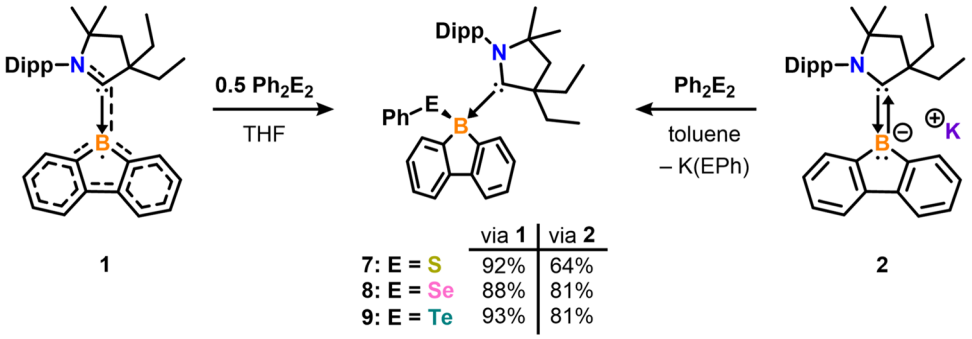

[a]Dashed lines in **1** represent delocalization of the radical across the ligand and boron heterocycle.

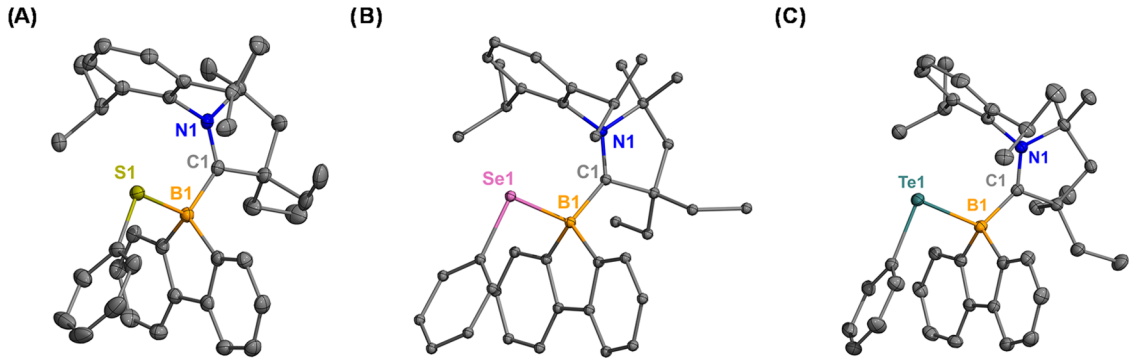

Figure 4. Molecular structures of **7** (A), **8** (B),[10] and **9** (C). H atoms omitted for clarity.

each disulfide bond, which are each close to 90° (Table S3). The slight degree of p_π overlap (Figure 3C,D), however, does result in π delocalization, and therefore slight bonding interactions, between nonadjacent sulfur atoms. The B1−S1−S1′−B1′ dihedral for compound **6** was determined to be −180.00(8)°, which results in direct overlap of the p_π lone pairs, leading to repulsion between the sulfur atoms and an elongated S−S bond (Figure 3E,F). This is further corroborated by IBO analysis, which shows a Wiberg bond order of 0.949. Despite the −180° torsion angle, the delocalization index of S1−S1′ (1.473) was calculated to be higher than that of S4−S4′ (1.162) in compound **3**, despite possessing similar dihedral angles. This can be attributed to the interatomic distance between S1−S1′ (2.0939(6) Å, **6**) when compared to S4−S4′ (2.267(7) Å, **3**).

Our observations of SET-based disulfide activation then led us to attempt the activation of diphenyl dichalcogenides with compounds **1** and **2**. The combination of 0.5 equiv of Ph_2S_2 with 1 equiv of **1** in THF gave a gradual color change from deep purple to colorless over the course of 2.5 h (Scheme 4). Subsequent removal of THF under vacuum gave compound **7** as a white powder in 92% yield. Under similar conditions, reactions of **1** with Ph_2Se_2 and Ph_2Te_2 led to immediate color changes from deep purple to yellow or orange. After a standard workup, compounds **8** and **9** were isolated as yellow and orange powders in 88 and 93% yield, respectively (Scheme 4). The $^{11}B\{^1H\}$ NMR resonances for **7**−**9** were observed at −5.1 ppm (**7**), −6.9 ppm (**8**), and −12.4 ppm (**9**), consistent with compounds containing tetracoordinate boron centers.[34] We then sought to test if compounds **7**−**9** could be formed from the reaction of the borafluorene anion **2** and Ph_2E_2 systems (Scheme 4). Because these reactions proceed with the concomitant formation of K(EPh), the isolated reaction yields are lower (**7**, 64%; **8**, 81%; **9**, 81%) due to the need to separate the coproduct. It should be noted that **8** has been previously reported by our lab, but was formed through a salt metathesis reaction by combining **2** and PhSeCl rather than through diselenide cleavage.[10]

Structural characterization of compounds **3**−**6** was conducted via single-crystal X-ray diffraction studies (Figure 4). As expected, the B−E (E = S, Se, Te) bond length (**7**: 1.972(2) Å, **8**: 2.103(7) Å, **9**: 2.335(2) Å) increases as the chalcogen size increases (Table 2). The B1−E1 bond length for **7**−**9** is

Table 2. Selected Bond Distances (Å) in Compounds 7−9

compd.	B1−E1	B1−C1	C1−N1
7 (S)	1.972(2)	1.650(2)	1.312(2)
8 (Se)	2.103(7)	1.634(7)	1.323(7)
9 (Te)	2.335(2)	1.621(3)	1.312(3)

indeed longer than the average B−E bond (1.915 Å for B−S, 2.055 for B−Se, 2.311 for B−Te), which can be attributed to the electron-rich nature of the boron center due to donation from the CAAC ligand. Consequently, the B1−C1 bond length (**7**: 1.650(2), **8**: 1.634(7), **9**: 1.621(3)) is inversely proportional to the B1−E1 distance.

To better understand the properties of compounds **7**−**9**, photophysical studies of (0.01 mM in THF) were performed (Figure 5 and Table 3). The λ_{max} for each compound is at approximately 320 nm. Compounds **7**−**9** each possess similar ultraviolet−visible (UV−vis) spectra. Density functional theory was employed to provide insight into the electronic structure of these species. All compounds were geometry optimized at the IEFPCM-SMD-THF-B3LYP-D3BJ/BS1 level of theory

https://doi.org/10.1021/acs.inorgchem.4c02459
Inorg. Chem. 2024, 63, 17639−17650

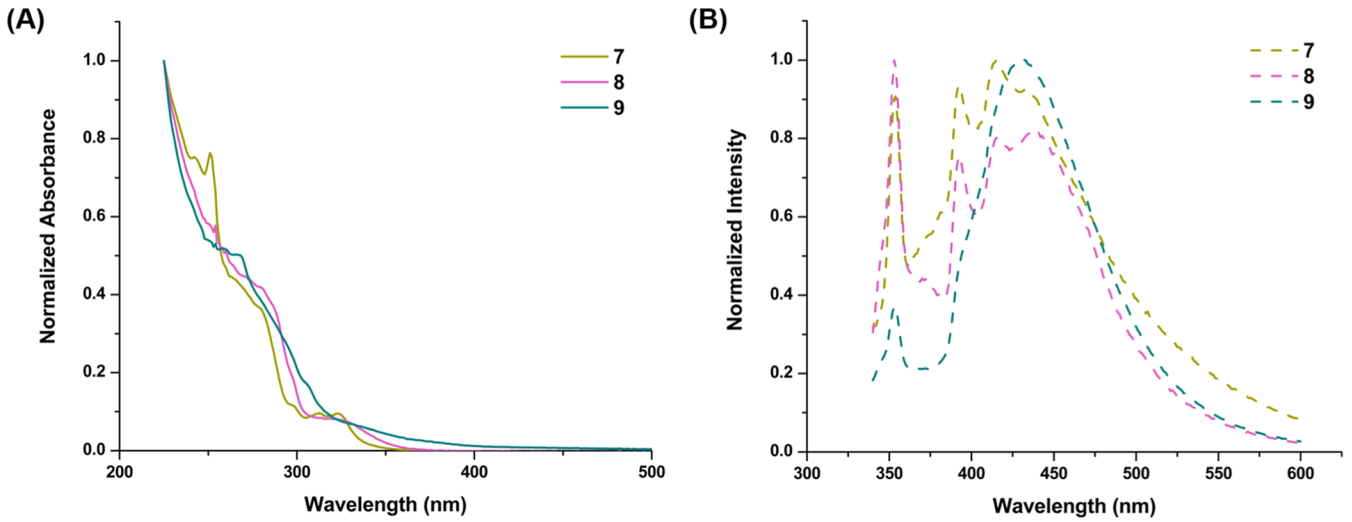

Figure 5. (A) Normalized UV−vis spectra and (B) fluorescence spectra for compounds for compounds **7** (yellow), **8** (pink), and **9** (green) (0.01 mM in THF; λ_{ex} = 320 nm at room temperature).

Table 3. Summary of Photophysical Data for Compounds 7−9

	7	8	9
λ_{max}[a]	320 nm	320 nm	320 nm
λ_{LE}[a]	436 nm	436 nm	431 nm
τ_1[b]	0.25 ns (24.75%)	0.22 ns (17.03%)	0.63 ns (26.49%)
τ_2[b]	4.73 ns (40.62%)	4.84 ns (40.22%)	4.27 ns (50.13%)
τ_3[b]	42.68 ns (34.62%)	29.33 ns (42.76%)	20.01 ns (23.39%)
χ^2	1.117	1.098	1.208

[a]0.01 mM in THF. [b]Fluorescence lifetime measurements collected at absorbance values below 0.1 (0.001 mM in THF) using time-correlated single photon counting (TCSPC).

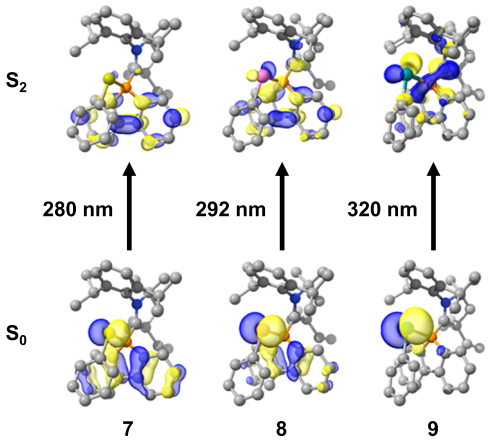

Figure 6. Natural transition orbitals for $S_0 \rightarrow S_2$ transition for compounds **7−9** computed at the IEFPCM-SMD-THF-TD-CAM-B3LYP-D3BJ//IEFPCM-SMD-THF-B3LYP-D3BJ/BS1 level of theory.

(BS1 = 6-31G(d) for H, B, C, N;[87−90] def2SVP for S, Se, Te).[91,92] Subsequent time-dependent density functional theory (TD-DFT) single point computations at the IEFPCM-SMD-THF-TD-CAM-B3LYP-D3BJ//IEFPCM-SMD-THF-B3LYP-D3BJ/BS1 level of theory were used to determine the nature of the lowest energy excitation for each compound (Figures S24−S29 and Tables S4−S6).[93−97] The $S_0 \rightarrow S_1$ transition for compounds **7−9** can be described by a $p_{chalcogen} \rightarrow \pi^*_{CAAC}$ transition, which is primarily HOMO → LUMO in nature. However, this transition is of Laporte forbidden $n \rightarrow \pi^*$ character, resulting in a low oscillator strength (f > 0.003). Therefore, the $S_0 \rightarrow S_2$ transition is predicted to be the lowest energy observable electronic transition, which is primarily $\pi^*_{CAAC} \rightarrow p_{chalcogen}/\pi_{borafluorene}$ in nature (Figure 6). These data are comparable to those computed at the the IEFPCM-SMD-THF-TD-CAM-B3LYP-D3BJ//IEFPCM-SMD-THF-TD-B3LYP-D3BJ/BS1 level of theory (Figures S36−S41, Tables S10−S12). As the chalcogen size is increased from S to Se to Te, the contribution of the chalcogen to the HOMO of each molecule increases (**7**: 43%, **8**: 56%, **9**: 75%) (Figure S48).

Time-dependent optimizations were performed at the TD-IEFPCM-SMD-THF-B3LYP-D3BJ/BS1 level of theory to model the excited state of compounds **7−9**. The excited state structures of these systems are different than that of the ground state (Kabsch RMSD = 0.393 Å (**7**), 0.453 Å (**8**), 0.280 Å (**9**))[98,99] (Figures S52−S54), which is experimentally corroborated by the difference in absorption and emission spectra as dictated by the Franck−Condon principle. Each compound possesses a similar emissive process at approximately 430 nm, which is attributable to emission from the CAAC π^* orbital (Figures S30−S35 and Tables S7−S9). Although a lower energy emissive process was computed for compounds **7−9**, the oscillator strength was significantly low (f > 0.002 for each compound) as a result of a forbidden $\pi^* \rightarrow n$ transition. It is predicted that the lowest energy emission process observable experimentally is the $S_2 \rightarrow S_0$ transition. Fluorescence lifetimes of compounds **7−9** were calculated using the time-correlated single photon counting (TCSPC) method monitored at 440 nm. It was observed that the fluorescence lifetimes of compounds **7−9** each possess a triexponential decay (Table 3). The third lifetime of compound **7** (42.68 ns) is longer than that of both compounds **8** (29.33 ns) and **9** (20.01 ns) (Table 3), which may be explained by consideration of an internal heavy atom effect,[100−103] whereby larger spin−orbit coupling (Te > Se > S) results in a decrease in fluorescence lifetime.

https://doi.org/10.1021/acs.inorgchem.4c02459
Inorg. Chem. 2024, 63, 17639−17650

CONCLUSIONS

We report the activation of elemental sulfur by the 9-CAAC-9-borafluorene radical (**1**) and anion (**2**), which proceed via a single-electron transfer mechanisms to form compounds containing sulfur-linked borafluorene units of varying length. The chain length was shortened from S_8 to S_7 by carbene-promoted sulfur extrusion via 1,3,4,5-tetramethylimidazol-2-ylidene (IMe_4). Compounds **1** and **2** were then used to activate disulfide, diselenide, and ditelluride bonds from their respective diphenyl dichalcogenides to form boryl chalcogenide compounds **7**–**9**. This study showcases the ability of CAAC-stabilized borafluorene radical and monoanion to facilitate dichalcogen bond cleavage. This SET mode of activation is currently being explored in our laboratory for the activation of a variety of small molecules (e.g., N_2O, CO, O_2).

EXPERIMENTAL SECTION

General Procedures. All air- and moisture-sensitive reactions were carried out under an inert atmosphere of argon using standard Schlenk techniques or in an MBRAUN LABmaster glovebox equipped with a −37 °C freezer. Reaction solvents, including toluene and hexanes were purified by distillation over sodium. Diethyl ether and tetrahydrofuran were purified via distillation over Na/benzophenone. Deuterated benzene and THF were purchased from Cambridge Isotope Laboratories. Deuterated benzene was dried by distilled over sodium/benzophenone and deuterated THF was dried by degassing, followed by stirring over sodium/potassium alloy (NaK) and filtering with a 0.45 μm PTFE syringe filter. All reaction glassware was oven-dried overnight at 190 °C. ^{1}H NMR spectra were collected on Bruker Avance III 600 MHz, Varian 600 MHz, or Bruker Avance NEO 400 MHz, or Bruker Avance-III HD Nanobay 400 MHz spectrometers. ^{11}B NMR spectra were collected on Bruker Avance NEO 400 MHz or Bruker Avance-III HD Nanobay 400 MHz spectrometers. ^{13}C NMR was collected on Bruker Avance III 800 MHz, Bruker Avance NEO 400 MHz, or Bruker Avance-III HD Nanobay 400 MHz spectrometers. 2D NMR were collected on Bruker Avance III 800 MHz and Bruker Avance-III HD Nanobay 400 MHz spectrometers. NMR signals are reported in parts per million (ppm) and referenced to residual solvent peaks in the deuterated solvent (^{1}H: C_6D_6 δ 7.16; THF-d_8 δ 3.58, 1.72; ^{13}C: C_6D_6 δ 128.06; THF-d_8 δ 67.21, 25.31). All boron signals are reported in ppm and were referenced to $BF_3{\cdot}Et_2O$ (^{11}B: δ = 0.0) following the standards and procedures established by IUPAC[104] using the unified scale approach. UV−vis data were collected on a Cary 60 UV−vis spectrometer, and samples were held in 1 cm square quartz cuvettes. Fluorescence and fluorescence lifetime data were collected using an Edinburgh Instruments FS5 Spectrofluorometer. Solutions were prepared in THF at 0.001 mM for fluorescence lifetime. A suspension of Ludox (colloidal silica) in deionized water was used to measure the instrument response factor (IRF). Lifetime fitting was performed using the Fluorophore software with χ^2 values between 0.8−1.5 with the smallest number of components being used for each fit. Single crystal X-ray diffraction data were collected on a Bruker Kappa APEXII Duo system equipped with a fine-focus sealed tube (Mo Kα, λ = 0.71073 Å, Cu Kα = 1.5406 Å). Single crystal X-ray diffraction data collection and structure refinement details are given in the X-ray crystallographic section. High resolution mass spectrometry (HRMS) was collected on a JEOL AccuTOF 4G LC-plus equipped with an ionSense DART (Direct Analysis in Real Time) source. The following compounds were prepared according to literature procedures: **1**,[31] **2**,[10] and IMe_4.[71] S_8 was purchased from Strem Chemicals and recrystallized from THF before use. Diphenyl disulfide was purchased from Aldrich Chemical Co. and recrystallized from hot MeOH before use. Diphenyl diselenide and diphenyl ditelluride were purchased from Aldrich Chemical Co. and used without further purification.

Compound ***3*** *(*^{Et}*CAAC-BF−*S_8*−BF-*^{Et}*CAAC).* In a 250 mL round-bottom flask, S_8 (137 mg, 0.535 mmol) was added to **1** (510 mg, 1.07 mmol) in 60 mL Et_2O. After several minutes, an off-white suspension began to form, and the reaction was left to stir at room temperature for 2 h. The off-white solid was collected via vacuum filtration and washed with 50 mL Et_2O to yield Compound **3** as an off-white solid (422 mg, 0.70 mmol, 65%). Single, colorless crystals of compound **3** were grown from THF/hexanes at −37 °C.

^{1}H NMR (400 MHz, C_6D_6) δ 7.87 (d, J = 7.4 Hz, 4H, BF−Ar*H*), 7.77 (d, J = 7.3 Hz, 4H, BF−Ar*H*), 7.38 (t, J = 7.3 Hz, 4H, BF−Ar*H*), 7.32 (t, J = 7.3 Hz, 4H, BF−Ar*H*), 7.12 (t, J = 7.7 Hz, 2H, ^{Et}CAAC−Ar*H** slight overlap with C_6D_6), 7.03 (d, J = 7.8 Hz, 4H, ^{Et}CAAC−Ar*H*), 3.03 (h, J = 6.0 Hz, 4H, ^{Et}CAAC−$(CH_3)_2CH$), 1.85 (d, J = 6.5 Hz, 12H, ^{Et}CAAC−CH$(CH_3)_2$), 1.46 (p, J = 7.5 Hz, 4H, ^{Et}CAAC−$(CH_3)CH_2$), 1.37 (s, 4H, ^{Et}CAAC−CH_2), 1.32 (p, J = 7.4 Hz, 4H, ^{Et}CAAC−$(CH_3)CH_2$), 1.20 (d, J = 6.4 Hz, 12H, ^{Et}CAAC−CH$(CH_3)_2$), 0.82 (s, 12H, ^{Et}CAAC−CH_3), 0.42 (t, J = 7.3 Hz, 12H, ^{Et}CAAC−$(CH_2)CH_3$). ^{13}C NMR (101 MHz, C_6D_6) δ 150.39 (^{Et}CAAC−Ar*C*), 146.26 (^{Et}CAAC−Ar*C*), 132.97 (BF−Ar*C*H), 131.25 (^{Et}CAAC−Ar*C*H), 127.00 (BF−Ar*C*H), 126.16 (BF−Ar*C*H), 125.98 (^{Et}CAAC−Ar*C*H), 119.90 (BF−Ar*C*H), 79.02 (^{Et}CAAC−*C*), 62.91 (^{Et}CAAC−$(CH_3)_2C$), 41.30 (^{Et}CAAC−CH_2), 34.07 (^{Et}CAAC−$(CH_3)_2CH_2$), 29.68 (^{Et}CAAC−$(CH_3)_2CH$), 28.94 (^{Et}CAAC−CH_3), 28.41 (^{Et}CAAC−CH$(CH_3)_2$), 25.68 (^{Et}CAAC−CH$(CH_3)_2$), 11.32 (^{Et}CAAC−$(CH_2)CH_3$). ^{11}B{^{1}H} NMR (128 MHz, C_6D_6) δ −4.6.

Compound ***4*** *(*^{Et}*CAAC-BF−*S_7*−BF-*^{Et}*CAAC).* From Compound **2**: In a vial, S_8 (50 mg, 0.19 mmol) was added to a solution of **2** (100 mg, 0.19 mmol) in Et_2O (15 mL). The reaction changed from dark red → purple → brown → yellow over the course of several minutes. The reaction was left to stir at room temperature for 16 h. The next day, the yellow-orange suspension was filtered, resulting in a yellow-orange solid and pale-yellow solution. The solid was dissolved in minimal THF, and a small amount of colorless single crystals of **4** were grown from THF/pentane vapor diffusion.

From Compound **3**: To a solution of IMe_4 (13 mg, 0.11 mmol) in toluene (10 mL), **3** (121 mg, 0.10 mmol) was added in one portion, which resulted in the immediate formation of a brown solution with white precipitate. The reaction was stirred at room temperature for 2 h before filtering and washing the resulting solid with 15 mL toluene. Compound **4** was isolated as a white solid (34 mg, 0.03 mmol, 29%).

^{1}H NMR (400 MHz, C_6D_6) δ 7.92 (d, J = 7.5 Hz, 4H, BF−Ar*H*), 7.75 (d, J = 7.4 Hz, 4H, BF−Ar*H*), 7.37 (t, J = 7.3 Hz, 4H, BF−Ar*H*), 7.26 (t, J = 7.2 Hz, 4H, BF−Ar*H*), 7.11 (t, 3H, ^{Et}CAAC−Ar*H** slight overlap with C_6D_6), 7.01 (d, J = 7.7 Hz, 4H, ^{Et}CAAC−Ar*H**), 3.00 (h, J = 6.9 Hz, 4H, ^{Et}CAAC−$(CH_3)_2CH$), 1.81 (d, J = 6.5 Hz, 12H, ^{Et}CAAC−CH$(CH_3)_2$), 1.45 (p, J = 7.6 Hz, 5H, ^{Et}CAAC−(CH_3)-CH_2), 1.36 (s, 4H, ^{Et}CAAC−CH_2), 1.31 (p, 4H, ^{Et}CAAC−CH_2), 1.24 (d, J = 6.3 Hz, 12H, ^{Et}CAAC−CH$(CH_3)_2$), 0.84 (s, 12H, ^{Et}CAAC−CH_3), 0.40 (t, J = 7.3 Hz, 12H, ^{Et}CAAC−$(CH_2)CH_3$). δ ^{13}C NMR (101 MHz, C_6D_6) 150.00 (^{Et}CAAC−Ar*C*), 145.69 (^{Et}CAAC−Ar*C*), 132.70 (BF−Ar*C*H), 131.03 (^{Et}CAAC−Ar*C*H), 126.52 (BF−Ar*C*H), 125.95 (BF−Ar*C*H), 125.65 (^{Et}CAAC−Ar*C*H), 119.33 (BF−Ar*C*H), 78.52 (^{Et}CAAC−*C*), 62.43 (^{Et}CAAC−$(CH_3)_2C$), 40.98 (^{Et}CAAC−CH_2), 33.70 (^{Et}CAAC−$(CH_3)_2CH_2$), 29.28 (^{Et}CAAC−*C*), 28.55 (^{Et}CAAC−$(CH_3)_2CH$), 27.77 (^{Et}CAAC−CH_3), 25.39 (^{Et}CAAC−CH$(CH_3)_2$), 10.94 (^{Et}CAAC−$(CH_2)CH_3$). δ ^{11}B{^{1}H} (128 MHz, C_6D_6) −5.4.

General Procedures for Compounds ***5*** *(*^{Et}*CAAC-BF−*S_2*−BF-*^{Et}*CAAC) and* ***6*** *(*^{Et}*CAAC-BF−*S_4*−BF-*^{Et}*CAAC).* In a vial, S_8 (x equiv, x = 1 for **5**; x = 0.5 for **6**) was added to 1 equiv of **2** in 10 mL THF. The color immediately changed from maroon → purple → yellow → red for both reactions. Single crystals were grown from slow evaporation of THF/hexanes for **5** and concentrated THF for **6**, respectively. Due to the complex mixture of products obtained, neither product was able to be characterized by NMR spectroscopy.

Compound ***7*** *(*^{Et}*CAAC-BF−SPh).* From Compound **1**: In a vial, Ph_2S_2 (4.4 mg, 0.02 mmol) was added to **1** (20 mg. 0.04 mmol) in 2 mL THF. Over the course of 2.5 h, the reaction color changed from deep purple to colorless. THF was then removed with vacuum to give Compound **7** as a white solid (22 mg, 92%). Colorless, single crystals

https://doi.org/10.1021/acs.inorgchem.4c02459
Inorg. Chem. 2024, 63, 17639−17650

of Compound **7** were grown from concentrated THF at room temperature.

From Compound **2**: In a vial, Ph_2S_2 (21 mg, 0.10 mmol) was added to **2** (52 mg, 0.10 mmol) in 7 mL toluene. The color gradually changed from deep maroon to lavender. After 3 h, the resulting white suspension was filtered through a 0.45 μM syringe filter and dried under vacuum, giving a **7** as a white solid (38 mg, 64%).

^{1}H NMR (600 MHz, C_6D_6) δ 7.86 (d, J = 7.2 Hz, 2H, BF−Ar*H*), 7.40 (d, J = 7.5 Hz, 2H, BF−Ar*H*), 7.29 (t, J = 7.2 Hz, 2H, BF−Ar*H*), 7.18 (t, J = 7.0 Hz, 3H, BF−Ar*H* and ^{Et}CAAC−Ar*H*), 7.09 (d, J = 7.6 Hz, 2H, ^{Et}CAAC−Ar*H* slight overlap with C_6D_6), 6.62 (dq, J = 6.0, 2.9 Hz, 1H, SPh−Ar*H*), 6.57−6.49 (m, 4H, SPh−Ar*H*), 3.17 (h, J = 6.6 Hz, 2H, ^{Et}CAAC−$(CH_3)_2CH$), 2.11 (d, J = 6.6 Hz, 6H, ^{Et}CAAC−$CH(CH_3)_2$), 1.48 (p, J = 7.4 Hz, 2H. ^{Et}CAAC−$(CH_3)CH_2$), 1.37 (s, 2H, ^{Et}CAAC−CH_2), 1.33 (p, J = 7.4 Hz, 2H, ^{Et}CAAC−$(CH_3)CH_2$), 1.23 (d, J = 6.4 Hz, 6H, ^{Et}CAAC−$CH(CH_3)_2$), 0.85 (s, 6H, ^{Et}CAAC−CH_3), 0.38 (t, J = 7.5 Hz, 6H, ^{Et}CAAC−$(CH_2)CH_3$). δ ^{13}C (201 MHz, C_6D_6) 149.47 (^{Et}CAAC−Ar*C*), 146.44 (BF−Ar*C*H or ^{Et}CAAC−Ar*C*H), 138.43 (SPh−Ar*C*), 136.24 (SPh−Ar*C*H), 133.74 (^{Et}CAAC−Ar*C*H), 132.86 (BF−Ar*C*H), 130.55 (BF−Ar*C*H), 129.45 (Ar*C*), 128.47 (Ar*C*), 126.50 (SPh−*Ar*CH), 126.25 (BF−Ar*C*H or ^{Et}CAAC−Ar*C*H), 125.75 (BF−Ar*C*H), 125.62 (^{Et}CAAC−Ar*C*H), 124.62 (SPh−*Ar*CH), 119.67 (BF−Ar*C*H), 79.21 (^{Et}CAAC−*C*), 63.18 (^{Et}CAAC−$(CH_3)_2C$), 41.36 (^{Et}CAAC−CH_2), 34.32 (^{Et}CAAC−$(CH_3)_2CH_2$), 29.91 (^{Et}CAAC−$(CH_3)_2CH$), 29.12 (^{Et}CAAC−CH_3), 28.44 (^{Et}CAAC−$CH(CH_3)_2$), 25.76 (^{Et}CAAC−$CH(CH_3)_2$), 11.49 (^{Et}CAAC−$(CH_2)CH_3$). ^{11}B{^{1}H} NMR (192 MHz, C_6D_6) δ −5.08. HRMS (AccuTof): calcd. $[C_{40}H_{48}BNS]$, m/z = 585.35950; found: m/z = 585.36456

Compound ***8*** *(^{Et}CAAC-BF−SePh).* From Compound **1**: In a vial, Ph_2Se_2 (6.2 mg, 0.02 mmol) was added to **1** (20 mg, 0.04 mmol) in 2 mL THF. The color immediately changed from purple to yellow. After 2.5 h, the yellow solution was dried under vacuum, giving Compound **8** as a yellow solid (23 mg, 88%).

From Compound **2**: In a vial, Ph_2Se_2 (31 mg, 0.10 mmol) was added to **2** (52 mg, 0.10 mmol) in 5 mL toluene. The color immediately changed from deep maroon to yellow. After 30 min, the resulting yellow suspension filtered through a 0.45 μM syringe filter and dried under vacuum, giving **8** as a light-yellow solid. (51 mg, 0.81 mmol, 81%).

NMR spectra are consistent with those reported in the literature.[10]

Compound ***9*** *(^{Et}CAAC-BF−TePh).* From Compound **2**: In a vial, Ph_2Te_2 (8.2 mg, 0.02 mmol) was added to **1** (20 mg, 0.04 mmol) in 3 mL THF. The color immediately changed from purple to red-orange. After 2.5 h, the red solution was dried under vacuum, giving **9** as an orange solid (26 mg, 92%). Orange-yellow, single crystals of Compound **9** were grown from concentrated Et_2O at room temperature.

From Compound **2**: In a vial, Ph_2Te_2 (41 mg, 0.10 mmol) was added to **2** (52 mg, 0.10 mmol) in 5 mL toluene. The color immediately changed from deep maroon to red-orange. After 30 min, the red-orange suspension was filtered through a 0.45 μM syringe filter and dried under vacuum, giving **9** as a light orange solid. (55 mg, 0.81 mmol, 81%).

^{1}H NMR (400 MHz, THF) δ 7.64 (d, J = 7.4 Hz, 2H, BF−Ar*H*), 7.53 (t, J = 7.1 Hz, 1H, ^{Et}CAAC−Ar*H*), 7.46−7.38 (d, 2H, ^{Et}CAAC−Ar*H*), 6.99 (d, J = 7.5 Hz, 2H, BF−Ar*H*), 6.91 (t, J = 7.2 Hz, 2H, BF−Ar*H*), 6.80 (td, J = 7.3, 1.2 Hz, 2H, BF−Ar*H*), 6.68−6.59 (m, 1H, TePh−*H*), 6.22 (t, J = 7.5 Hz, 2H, TePh−*H*), 6.15 (d, J = 7.4 Hz, 2H, TePh−*H*), 3.26 (hept, J = 6.5 Hz, 2H, ^{Et}CAAC−$(CH_3)_2CH$), 2.09 (s, 2H, ^{Et}CAAC−CH_2), 2.07 (d, J = 6.4 Hz, 6H, ^{Et}CAAC−$CH(CH_3)_2$) 1.50 (s, 6H, ^{Et}CAAC−CH_3), 1.47 (d, J = 6.4 Hz, 6H, ^{Et}CAAC−$CH(CH_3)_2$), 1.35−1.19 (p, 4H, ^{Et}CAAC−$(CH_3)CH_2$), 0.65 (t, J = 7.5 Hz, 6H, ^{Et}CAAC−$CH_2(CH_3)_2$). δ ^{13}C (101 MHz, THF) 148.00 (^{Et}CAAC−Ar*C*), 147.42 (^{Et}CAAC−Ar*C*), 142.00 (TePh−Ar*C*H), 133.42 (BF−Ar*C*H), 131.59 (^{Et}CAAC−Ar*C*H), 127.29 (^{Et}CAAC−Ar*C*H), 126.36 (TePh−Ar*C*H), 125.56 (BF−Ar*C*H), 125.23 (BF−Ar*C*H), 125.04 (TePh−Ar*C*H), 119.66 (TePh−Ar*C*H), 114.33 (Ar*C*), 81.05 (^{Et}CAAC−*C*), 64.88 (^{Et}CAAC−$(CH_3)_2C$), 42.61 (^{Et}CAAC−$CH(CH_3)_2$), 34.93 (^{Et}CAAC−$(CH_3)_2CH_2$), 30.58 (^{Et}CAAC−$(CH_3)_2CH$), 29.95 (^{Et}CAAC−CH_3), 29.09 (^{Et}CAAC−$(CH_3)_2CH$), 26.84 (^{Et}CAAC−$(CH_3)_2CH$), 11.51 (^{Et}CAAC−$(CH_2)CH_3$). ^{11}B{^{1}H} NMR (192 MHz, C_6D_6) δ −12.4. HRMS (AccuTof): calcd. $[C_{40}H_{47}BNTe]^+$, m/z = 682.29074; found: m/z = 682.28693

Computational Details. All density functional theory computations were carried out using Gaussian 16 Revision C.01,[105] using the default pruned UltraFine grids using 99 radial shells with 590 points per shell (99,590) and pruned SG1 grids using 50 radial shells with 194 points per shell (50,194) for Hessians. Default convergence for the SCF (10^{-8}) were used. All structures were optimized at the IEFPCM-SMD-THF-B3LYP-D3BJ/BS1 level of theory (BS1 = 6-31G(d) for H, B, C, N;[87−90] def2SVP for S, Se, Te[91,92]) The IEFPCM-SMD solvation model[96,97] was used for all computations to employ parameters consistent with the use of tetrahydrofuran as the solvent. To confirm that each stationary point was a minimum or transition state, analytical frequency computations were performed at the same level of theory. Time-dependent DFT (TD-DFT)[106] geometry optimizations and corresponding harmonic vibrational frequencies were computed by solving iteratively for the first 5 singlet excitations [TD(ROOT = 1,NSTATES = 5)] (TD-IEFPCM-SMD-B3LYP-D3BJ/BS1), after which the first singlet excited states were optimized using analytical gradients. To simulate absorption and emission spectra using TD-DFT, the first 20 vertical transitions were computed for corresponding optimized geometries of each compound with (TD-IEFPCM-SMD-CAM-B3LYP//IEFPCM-SMD-B3LYP-D3BJ/BS1) for absorption and (TD-IEFPCM-SMD-CAM-B3LYP//TD-IEFPCM-SMD-B3LYP-D3BJ/BS1) for emission.[107] Simulated spectra were obtained using GaussSum 3.0[108] with a fwhm of 2000 cm^{-1}. Natural transition orbitals (NTOs) were visualized using ChimeraX[109−111] with a contour value of 0.05. Intrinsic bond orbitals (IBOs) and Wiberg Bond Indices (WBI) were computed on solid state structures of compounds **3**−**6** by first running single point calculations on the solid-state structure of each compound at the B3LYP-D3BJ/def2SVP[91] level of theory using ORCA 5.0,[112] followed by computing the molecular orbital localization within IboView[113] using IBO (exponent 2). IBOs were visualized using IboView.[113] Delocalization indices were computed on solid state structures of compounds **3**−**6** by first running single point calculations on the solid-state structure of each compound at the B3LYP-D3BJ/def2SVP[91] level of theory using ORCA 5.0,[112] and then computing the indices using Multiwfn 3.8.[114] Kabsch RMSD values were computed using the "Calculate Root-mean-square deviation (RMSD) of Two Molecules Using Rotation" Python script.[98,99] Overlaid structures of compounds **7**−**9** were visualized using Jimp2.[115]

■ ASSOCIATED CONTENT

Supporting Information

The Supporting Information is available free of charge at https://pubs.acs.org/doi/10.1021/acs.inorgchem.4c02459.

NMR spectra; X-ray refinement details; and computational data (PDF)

Accession Codes

CCDC 2353540−2353545 contain the supplementary crystallographic data for this paper. These data can be obtained free of charge via www.ccdc.cam.ac.uk/data_request/cif, or by emailing data_request@ccdc.cam.ac.uk, or by contacting The Cambridge Crystallographic Data Centre, 12 Union Road, Cambridge CB2 1EZ, U.K.; fax: +44 1223 336033.

■ AUTHOR INFORMATION

Corresponding Authors

Charles Edwin Webster − *Department of Chemistry, Mississippi State University, Mississippi State, Mississippi*

https://doi.org/10.1021/acs.inorgchem.4c02459
Inorg. Chem. 2024, 63, 17639−17650

39762, United States; orcid.org/0000-0002-6917-2957; Email: ewebster@chemistry.msstate.edu
Robert J. Gilliard, Jr. − *Department of Chemistry, Massachusetts Institute of Technology, Cambridge, Massachusetts 02139-4307, United States;* orcid.org/0000-0002-8830-1064; Email: gilliard@mit.edu

Authors

Nathan C. Frey − *Department of Chemistry, Massachusetts Institute of Technology, Cambridge, Massachusetts 02139-4307, United States;* orcid.org/0000-0001-7406-1736
Kimberly K. Hollister − *Department of Chemistry, Massachusetts Institute of Technology, Cambridge, Massachusetts 02139-4307, United States;* orcid.org/0000-0001-9024-4436
Peter Müller − *Department of Chemistry, Massachusetts Institute of Technology, Cambridge, Massachusetts 02139-4307, United States;* orcid.org/0000-0001-6530-3852
Diane A. Dickie − *Department of Chemistry, University of Virginia, Charlottesville, Virginia 22904, United States;* orcid.org/0000-0003-0939-3309

Complete contact information is available at: https://pubs.acs.org/10.1021/acs.inorgchem.4c02459

Notes

The authors declare no competing financial interest.

■ ACKNOWLEDGMENTS

The authors acknowledge the National Science Foundation Chemical Synthesis (CHE-2046544), Chemical Catalysis (CHE-2102552), and Major Research Instrumentation (CHE-2018870) programs for support of this work. R.J.G. acknowledges additional laboratory support from the Arnold and Mabel Beckman Foundation through a Beckman Young Investigator Award. N.C.F. acknowledges the National Science Foundation for a Graduate Research Fellowship (grant #1842490). K.K.H. thanks the American Association of University Women for an American Dissertation Fellowship. C.E.W. acknowledges the use of resources provided by the Mississippi Center for Supercomputing Research (MCSR) at the University of Mississippi and the High Performance Computing Collaboratory (HPC^2) at Mississippi State University.

■ REFERENCES

(1) Segawa, Y.; Yamashita, M.; Nozaki, K. Boryllithium: Isolation, Characterization, and Reactivity as a Boryl Anion. *Science* **2006**, *314* (5796), 113−115.
(2) Yamashita, M.; Nozaki, K. Boryllithium: A novel boron nucleophile and its application in the synthesis of borylmetal complexes. *Pure Appl. Chem.* **2008**, *80* (5), 1187−1194.
(3) Yamashita, M. Nucleophilicity of a Base-Stabilized Borole Anion at the Boron Center. *Angew. Chem., Int. Ed.* **2010**, *49* (14), 2474−2475.
(4) Braunschweig, H.; Chiu, C.-W.; Radacki, K.; Kupfer, T. Synthesis and Structure of a Carbene-Stabilized π-Boryl Anion. *Angew. Chem., Int. Ed.* **2010**, *49* (11), 2041−2044.
(5) Budy, H.; Gilmer, J.; Trageser, T.; Wagner, M. Anionic Organoboranes: Delicate Flowers Worth Caring for. *Eur. J. Inorg. Chem.* **2020**, *2020* (44), 4148−4162.
(6) Protchenko, A. V.; Vasko, P.; Fuentes, M. Á.; Hicks, J.; Vidovic, D.; Aldridge, S. Approaching a "Naked" Boryl Anion: Amide Metathesis as a Route to Calcium, Strontium, and Potassium Boryl Complexes. *Angew. Chem., Int. Ed.* **2021**, *60* (4), 2064−2068.
(7) Yamashita, M.; Nozaki, K. Boryl Anions. In *Synthesis and Application of Organoboron Compounds*; Fernández, E., Whiting, A., Eds.; Springer International Publishing, 2015; pp 1−37.
(8) Saalfrank, C.; Fantuzzi, F.; Kupfer, T.; Ritschel, B.; Hammond, K.; Krummenacher, I.; Bertermann, R.; Wirthensohn, R.; Finze, M.; Schmid, P.; et al. cAAC-Stabilized 9,10-diboraanthracenes—Acenes with Open-Shell Singlet Biradical Ground States. *Angew. Chem., Int. Ed.* **2020**, *59* (43), 19338−19343.
(9) Hübner, A.; Qu, Z.-W.; Englert, U.; Bolte, M.; Lerner, H.-W.; Holthausen, M. C.; Wagner, M. Main-Chain Boron-Containing Oligophenylenes via Ring-Opening Polymerization of 9-H-9-Borafluorene. *J. Am. Chem. Soc.* **2011**, *133* (12), 4596−4609.
(10) Wentz, K. E.; Molino, A.; Weisflog, S. L.; Kaur, A.; Dickie, D. A.; Wilson, D. J. D.; Gilliard, R. J., Jr. Stabilization of the Elusive 9-Carbene-9-Borafluorene Monoanion. *Angew. Chem., Int. Ed.* **2021**, *60* (23), 13065−13072.
(11) Yamashita, M. Creation of Nucleophilic Boryl Anions and Their Properties. *Bull. Chem. Soc. Jpn.* **2011**, *84* (10), 983−999.
(12) Barker, J. E.; Obi, A. D.; Dickie, D. A.; Gilliard, R. J., Jr. Boron-Doped Pentacenes: Isolation of Crystalline 5,12- and 5,7-Diboratapentacene Dianions. *J. Am. Chem. Soc.* **2023**, *145* (4), 2028−2034.
(13) Jaramillo, P.; Pérez, P.; Fuentealba, P. On the Nucleophilicity of Boryllithium Compounds. A Theoretical Study. *J. Phys. Chem. A* **2009**, *113* (24), 6812−6817.
(14) Weber, L. 1,3,2-Diazaborolyl Anions − From Laboratory Curiosities to Versatile Reagents in Synthesis. *Eur. J. Inorg. Chem.* **2017**, *2017* (29), 3461−3488.
(15) Bertermann, R.; Braunschweig, H.; Dewhurst, R. D.; Hörl, C.; Kramer, T.; Krummenacher, I. Evidence for Extensive Single-Electron-Transfer Chemistry in Boryl Anions: Isolation and Reactivity of a Neutral Borole Radical. *Angew. Chem., Int. Ed.* **2014**, *53* (21), 5453−5457.
(16) Yamashita, M.; Nozaki, K. Recent Developments of Boryl Anions: Boron Analogues of Carbanion. *Bull. Chem. Soc. Jpn.* **2008**, *81* (11), 1377−1392.
(17) Kajiwara, T.; Terabayashi, T.; Yamashita, M.; Nozaki, K. Syntheses, Structures, and Reactivities of Borylcopper and -zinc Compounds: 1,4-Silaboration of an α,β-Unsaturated Ketone to Form a γ-Siloxyallylborane. *Angew. Chem., Int. Ed.* **2008**, *47* (35), 6606−6610.
(18) Yamashita, M.; Suzuki, Y.; Segawa, Y.; Nozaki, K. Synthesis, Structure of Borylmagnesium, and Its Reaction with Benzaldehyde to Form Benzoylborane. *J. Am. Chem. Soc.* **2007**, *129* (31), 9570−9571.
(19) Segawa, Y.; Yamashita, M.; Nozaki, K. Boryl Anion Attacks Transition-Metal Chlorides To Form Boryl Complexes: Syntheses, Spectroscopic, and Structural Studies on Group 11 Borylmetal Complexes. *Angew. Chem., Int. Ed.* **2007**, *46* (35), 6710−6713.
(20) Hollister, K. K.; Yang, W.; Mondol, R.; Wentz, K. E.; Molino, A.; Kaur, A.; Dickie, D. A.; Frenking, G.; Pan, S.; Wilson, D. J. D.; Gilliard, R. J. Isolation of Stable Borepin Radicals and Anions. *Angew. Chem., Int. Ed.* **2022**, *61* (23), No. e202202516.
(21) von Grotthuss, E.; Diefenbach, M.; Bolte, M.; Lerner, H.-W.; Holthausen, M. C.; Wagner, M. Reversible Dihydrogen Activation by Reduced Aryl Boranes as Main-Group Ambiphiles. *Angew. Chem., Int. Ed.* **2016**, *55* (45), 14067−14071.
(22) Wentz, K. E.; Molino, A.; Freeman, L. A.; Dickie, D. A.; Wilson, D. J. D.; Gilliard, R. J., Jr. Systematic Electronic and Structural Studies of 9-Carbene-9-Borafluorene Monoanions and Transformations into Luminescent Boron Spirocycles. *Inorg. Chem.* **2022**, *61* (43), 17049−17058.
(23) Wentz, K. E.; Molino, A.; Freeman, L. A.; Dickie, D. A.; Wilson, D. J. D.; Gilliard, R. J., Jr. Reactions of 9-Carbene-9-Borafluorene Monoanion and Selenium: Synthesis of Boryl-Substituted Selenides and Diselenides. *Inorg. Chem.* **2021**, *60* (18), 13941−13949.
(24) Su, Y.; Kinjo, R. Boron-containing radical species. *Coord. Chem. Rev.* **2017**, *352*, 346−378.
(25) Power, P. P. Persistent and Stable Radicals of the Heavier Main Group Elements and Related Species. *Chem. Rev.* **2003**, *103* (3), 789−810.

(26) Yuan, N.; Wang, W.; Wu, Z.; Chen, S.; Tan, G.; Sui, Y.; Wang, X.; Jiang, J.; Power, P. P. A boron-centered radical: a potassium-crown ether stabilized boryl radical anion. *Chem. Commun.* **2016**, *52* (86), 12714−12716.
(27) Bissinger, P.; Braunschweig, H.; Damme, A.; Krummenacher, I.; Phukan, A. K.; Radacki, K.; Sugawara, S. Isolation of a Neutral Boron-Containing Radical Stabilized by a Cyclic (Alkyl)(Amino)-Carbene. *Angew. Chem., Int. Ed.* **2014**, *53* (28), 7360−7363.
(28) Ueng, S.-H.; Solovyev, A.; Yuan, X.; Geib, S. J.; Fensterbank, L.; Lacôte, E.; Malacria, M.; Newcomb, M.; Walton, J. C.; Curran, D. P. N-Heterocyclic Carbene Boryl Radicals: A New Class of Boron-Centered Radical. *J. Am. Chem. Soc.* **2009**, *131* (31), 11256−11262.
(29) Sarkar, S. K.; Hollister, K. K.; Molino, A.; Obi, A. D.; Deng, C.-L.; Tra, B. Y. E.; Stewart, B. M.; Dickie, D. A.; Wilson, D. J. D.; Gilliard, R. J., Jr. Bis(9-Boraphenanthrene) and Its Stable Biradical. *J. Am. Chem. Soc.* **2023**, *145*, 21475−21482, DOI: 10.1021/jacs.3c07236.
(30) Xiang, L.; Wang, J.; Krummenacher, I.; Radacki, K.; Braunschweig, H.; Lin, Z.; Ye, Q. Persistent and Predominantly Localized Boron Radical from the Reduction of a Three-Dimensional Analogue of NHC-Stabilized Borafluorenium. *Chem. - Eur. J.* **2023**, *29* (42), No. e202301270.
(31) Yang, W.; Krantz, K. E.; Freeman, L. A.; Dickie, D. A.; Molino, A.; Frenking, G.; Pan, S.; Wilson, D. J. D.; Gilliard, R. J., Jr. Persistent Borafluorene Radicals. *Angew. Chem., Int. Ed.* **2020**, *59* (10), 3850−3854.
(32) Gilmer, J.; Budy, H.; Kaese, T.; Bolte, M.; Lerner, H.-W.; Wagner, M. The 9H-9-Borafluorene Dianion: A Surrogate for Elusive Diarylboryl Anion Nucleophiles. *Angew. Chem., Int. Ed.* **2020**, *59* (14), 5621−5625.
(33) Wentz, K. E.; Molino, A.; Freeman, L. A.; Dickie, D. A.; Wilson, D. J. D.; Gilliard, R. J., Jr. Approaching Dianionic Tetraoxadiborecine Macrocycles: 10-Membered Bora-Crown Ethers Incorporating Borafluorenate Units. *Angew. Chem., Int. Ed.* **2023**, *62* (5), No. e202215772.
(34) Su, X.; Bartholome, T. A.; Tidwell, J. R.; Pujol, A.; Yruegas, S.; Martinez, J. J.; Martin, C. D. 9-Borafluorenes: Synthesis, Properties, and Reactivity. *Chem. Rev.* **2021**, *121* (7), 4147−4192.
(35) Braunschweig, H.; Dellermann, T.; Ewing, W. C.; Kramer, T.; Schneider, C.; Ullrich, S. Reductive Insertion of Elemental Chalcogens into Boron−Boron Multiple Bonds. *Angew. Chem., Int. Ed.* **2015**, *54* (35), 10271−10275.
(36) Chen, P.; Cui, C. Isolable Boron Persulfide: Activation of Elemental Sulfur with a 2-Chloro-Azaborolyl Anion. *Chem. - Eur. J.* **2016**, *22* (9), 2902−2905.
(37) Auerhammer, D.; Arrowsmith, M.; Dewhurst, R. D.; Kupfer, T.; Böhnke, J.; Braunschweig, H. Closely related yet different: a borylene and its dimer are non-interconvertible but connected through reactivity. *Chem. Sci.* **2018**, *9* (8), 2252−2260.
(38) Liu, S.; Légaré, M.-A.; Hofmann, A.; Rempel, A.; Hagspiel, S.; Braunschweig, H. Synthesis of unsymmetrical B2E2 and B2E3 heterocycles by borylene insertion into boradichalcogeniranes. *Chem. Sci.* **2019**, *10* (17), 4662−4666.
(39) Chen, P.; Cui, C. Reactivity of the 2-Chloroazaborolyl Anion. *Eur. J. Inorg. Chem.* **2017**, *2017* (38−39), 4480−4484.
(40) Dietz, M.; Arrowsmith, M.; Gärtner, A.; Radacki, K.; Bertermann, R.; Braunschweig, H. Harnessing the electronic differences between CAAC-stabilised 1,4-diborabenzene and 9,10-diboraanthracene for synthesis. *Chem. Commun.* **2021**, *57* (99), 13526−13529.
(41) von Grotthuss, E.; Nawa, F.; Bolte, M.; Lerner, H.-W.; Wagner, M. Chalcogen−chalcogen-bond activation by an ambiphilic, doubly reduced organoborane. *Tetrahedron* **2019**, *75* (1), 26−30.
(42) Goh, G. K. H.; Li, Y.; Kinjo, R. Oxidative addition of elemental selenium to 1,4,2,5-diazadiborinine. *Dalton Trans.* **2019**, *48* (22), 7514−7518.
(43) Braunschweig, H.; Constantinidis, P.; Dellermann, T.; Ewing, W. C.; Fischer, I.; Hess, M.; Knight, F. R.; Rempel, A.; Schneider, C.; Ullrich, S.; et al. Highly Strained Heterocycles Constructed from Boron−Boron Multiple Bonds and Heavy Chalcogens. *Angew. Chem., Int. Ed.* **2016**, *55* (18), 5606−5609.
(44) Liu, S.; Légaré, M.-A.; Hofmann, A.; Braunschweig, H. A Boradiselenirane and a Boraditellurirane: Isolable Heavy Analogs of Dioxiranes and Dithiiranes. *J. Am. Chem. Soc.* **2018**, *140* (36), 11223−11226.
(45) Kundu, G.; Amrutha, P. R.; Tothadi, S.; Sen, S. S. Access to NHC−Boryl Mono- and Bis-Selenide and Utility as Mild Selenium Transfer Reagent including to the C−F Bond *Chem. - Eur. J., 30* 6 e202302984 .
(46) Liu, S.; Légaré, M.-A.; Auerhammer, D.; Hofmann, A.; Braunschweig, H. The First Boron−Tellurium Double Bond: Direct Insertion of Heavy Chalcogens into a Mn═B Double Bond. *Angew. Chem., Int. Ed.* **2017**, *56* (49), 15760−15763.
(47) Steudel, R. *Homocyclic Sulfur Molecules*; Springer: Berlin, Heidelberg, 1982; pp 149−176.
(48) Lee, M. H.; Yang, Z.; Lim, C. W.; Lee, Y. H.; Dongbang, S.; Kang, C.; Kim, J. S. Disulfide-Cleavage-Triggered Chemosensors and Their Biological Applications. *Chem. Rev.* **2013**, *113* (7), 5071−5109.
(49) Deng, Z.; Hu, J.; Liu, S. Disulfide-Based Self-Immolative Linkers and Functional Bioconjugates for Biological Applications. *Macromol. Rapid Commun.* **2020**, *41* (1), No. 1900531.
(50) Stasińska, A. R.; Putaj, P.; Chmielewski, M. K. Disulfide bridge as a linker in nucleic acids' bioconjugation. Part II: A summary of practical applications. *Bioorg. Chem.* **2020**, *95*, No. 103518.
(51) Northfield, S. E.; Wang, C. K.; Schroeder, C. I.; Durek, T.; Kan, M.-W.; Swedberg, J. E.; Craik, D. J. Disulfide-rich macrocyclic peptides as templates in drug design. *Eur. J. Med. Chem.* **2014**, *77*, 248−257.
(52) Guan, X. Glutathione and glutathione disulfide − their biomedical and pharmaceutical applications. *Med. Chem. Res.* **2023**, *32*, 1972−1994, DOI: 10.1007/s00044-023-03116-9.
(53) Manthiram, A.; Fu, Y.; Chung, S.-H.; Zu, C.; Su, Y.-S. Rechargeable Lithium−Sulfur Batteries. *Chem. Rev.* **2014**, *114* (23), 11751−11787.
(54) Wild, M.; O'Neill, L.; Zhang, T.; Purkayastha, R.; Minton, G.; Marinescu, M.; Offer, G. J. Lithium sulfur batteries, a mechanistic review. *Energy Environ. Sci.* **2015**, *8* (12), 3477−3494.
(55) Samuel, E. π-Complexes of Group IVA metals with cyclopentadiene, indene, and fluorene. *Bull. Soc. Chim. France* **1966**, *11*, 3548−3564.
(56) Suzuki, H.; Tokitoh, N.; Okazaki, R.; Nagase, S.; Goto, M. Synthesis, Structure, and Reactivity of the First Kinetically Stabilized Silanethione. *J. Am. Chem. Soc.* **1998**, *120* (43), 11096−11105.
(57) Groom, C. R.; Bruno, I. J.; Lightfoot, M. P.; Ward, S. C. The Cambridge Structural Database. *Acta Crystallogr., Sect. B: Struct. Sci., Cryst. Eng. Mater.* **2016**, *72* (2), 171−179.
(58) Cao, L. L.; Stephan, D. W. Homolytic Cleavage Reactions of a Neutral Doubly Base Stabilized Diborane(4). *Organometallics* **2017**, *36* (16), 3163−3170.
(59) Liu, L. L.; Cao, L. L.; Shao, Y.; Stephan, D. W. Single Electron Delivery to Lewis Pairs: An Avenue to Anions by Small Molecule Activation. *J. Am. Chem. Soc.* **2017**, *139* (29), 10062−10071.
(60) Schwamm, R. J.; Lein, M.; Coles, M. P.; Fitchett, C. M. Bismuth(III) Complex of the [S4]•− Radical Anion: Dimer Formation via Pancake Bonds. *J. Am. Chem. Soc.* **2017**, *139* (46), 16490−16493.
(61) Li, S.; Shiri, F.; Xu, G.; Yiu, S.-M.; Lee, H. K.; Ng, T. H.; Lin, Z.; Lu, Z. Reactivity of a Hexaaryldiboron(6) Dianion as Boryl Radical Anions. *J. Am. Chem. Soc.* **2024**, *146*, 17348−17354, DOI: 10.1021/jacs.4c04253.
(62) Bluer, K. R.; Laperriere, L. E.; Pujol, A.; Yruegas, S.; Adiraju, V. A. K.; Martin, C. D. Coordination and Ring Expansion of 1,2-Dipolar Molecules with 9-Phenyl-9-borafluorene. *Organometallics* **2018**, *37* (17), 2917−2927.
(63) Bischof, T.; Wieprecht, N.; Fuchs, S.; Endres, L.; Krummenacher, I.; Michel, M.; Mihm, C.; Braunschweig, H.; Finze, M. Unlocking Heteroaromatic Ring Systems through Chalcogen

Insertion into Boroles. *Inorg. Chem.* **2023**, *62*, 21329−21335, DOI: 10.1021/acs.inorgchem.3c03403.
(64) Tarasova, N. P.; Zanin, A. A.; Krivoborodov, E. G.; Mezhuev, Y. O. Elemental sulphur in the synthesis of sulphur-containing polymers: reaction mechanisms and green prospects. *RSC Adv.* **2021**, *11* (15), 9008−9020.
(65) Williams, C. R.; Harpp, D. N. Sulfur Extrusion Reactions - Scope and Mechanistic Aspects. *Sulfur Rep.* **1990**, *10* (2), 103−191.
(66) Harpp, D. N.; Gleason, J. G.; Snyder, J. P. Organic sulfur chemistry. I. The disulfide-phosphine reaction. Desulfurization with tris(diethylamino)phosphine. *J. Am. Chem. Soc.* **1968**, *90* (15), 4181−4182.
(67) Harpp, D. N.; Gleason, J. G. Organic sulfur chemistry. X. Selective desulfurization of disulfides. Scope and mechanism. *J. Am. Chem. Soc.* **1971**, *93* (10), 2437−2445.
(68) Harpp, D. N.; Smith, R. A. Organic sulfur chemistry. 42. Sulfur-sulfur bond cleavage processes. Selective desulfurization of trisulfides. *J. Am. Chem. Soc.* **1982**, *104* (22), 6045−6053.
(69) Galow, A. P.; Rominger, F.; Mastalerz, M. N-Heterocyclic Carbene Mediated Sulfur Extrusion of Disulfides. *Eur. J. Org. Chem.* **2023**, *26* (7), No. e202201383.
(70) Tran, P. M.; Wang, Y.; Xie, Y.; Wei, P.; Lahm, M. E.; Schaefer, H. F., III; Robinson, G. H. Phosphine-Mediated Cleavage of Sulfur−Sulfur Bonds. *Organometallics* **2022**, *41* (22), 3099−3103.
(71) Kuhn, N.; Kratz, T. Synthesis of Imidazol-2-ylidenes by Reduction of Imidazole-2(3H)-thiones. *Synthesis* **1993**, *1993* (06), 561−562.
(72) Müller, A.; Römer, M.; Bögge, H.; Krickemeyer, E.; Baumann, F.-W.; Schmitz, K. (PPh4)4[Ag2S20]·S8, an unusual very sulfur-rich compound. *Inorg. Chim. Acta* **1984**, *89* (1), L7−L8.
(73) Müller, A.; Baumann, F.-W.; Bögge, H.; Römer, M.; Krickemeyer, E.; Schmitz, K. Novel Inorganic Ring Systems and Fixation of the S Ion:[(S6)Cu(S8)Cu(S6)]4⊖ and [Cu3(S4)3]3⊖. *Angew. Chem., Int. Ed.* **1984**, *23* (8), 632−633.
(74) Rybak, W. K.; Cymbaluk, A.; Siczek, M.; Skonieczny, J. Crystallization-Induced Asymmetric Synthesis of Nonracemic Platinum(IV) Polysulfide Tris(chelate) Complexes. *Eur. J. Inorg. Chem.* **2012**, *2012* (23), 3675−3679.
(75) Dev, S.; Ramli, E.; Rauchfuss, T. B.; Wilson, S. R. Synthesis and structure of [M(N-methylimidazole)6]S8 (M = manganese, iron, nickel, magnesium). Polysulfide salts prepared by the reaction N-methylimidazole + metal powder + sulfur. *Inorg. Chem.* **1991**, *30* (11), 2514−2519.
(76) Liebing, P.; Kühling, M.; Swanson, C.; Feneberg, M.; Hilfert, L.; Goldhahn, R.; Chivers, T.; Edelmann, F. T. Catenated and spirocyclic polychalcogenides from potassium carbonate and elemental chalcogens. *Chem. Commun.* **2019**, *55* (99), 14965−14967.
(77) Mondal, M. K.; Zhang, L.; Feng, Z.; Tang, S.; Feng, R.; Zhao, Y.; Tan, G.; Ruan, H.; Wang, X. Tricoordinate Nontrigonal Pnictogen-Centered Radical Anions: Isolation, Characterization, and Reactivity. *Angew. Chem., Int. Ed.* **2019**, *58* (44), 15829−15833.
(78) Krebs, H.; Müller, K.-H. Darstellung und Eigenschaften von Wasserstoffpolysulfiden organischer Basen. II. *Z. Anorg. Allg. Chem.* **1955**, *281* (3−4), 187−189.
(79) Steudel, R.; Pridöhl, M.; Buschmann, J.; Luger, P. Synthesis of Bis(trichloromethyl)tetra- and -heptasulfane from Titanocene Polysulfide Complexes and Structure of (CCl3)2S7. *Chem. Ber.* **1995**, *128* (7), 725−728.
(80) Chivers, T.; Edelmann, F.; Richardson, J. F.; Schmidt, K. J. Convenient synthesis, X-ray crystal structure, and Raman spectrum of the heptasulphide dianion, S72−, in [PPN]2S7•2EtOH. *Can. J. Chem.* **1986**, *64* (8), 1509−1513.
(81) Müller, A.; Krickemeyer, E.; Zimmermann, M.; Römer, M.; Bögge, H.; Penk, M.; Schmitz, K. [Ag2(S6)2]2- (with a novel cyclic inorganic ring system), [Ag(S9)]- and (PPh4)(NH4)S7·CH3CN with an unusual conformation of the heptasulfide ion. *Inorg. Chim. Acta* **1984**, *90* (3), L69−L71.
(82) Kanatzidis, M. G.; Baenziger, N. C.; Coucouvanis, D. Crystal structure determination of bis(tetraphenylphosphonium) heptasulfide, (Ph4P)2S7. *Inorg. Chem.* **1983**, *22* (2), 290−292.
(83) Dhingra, S. S.; Kanatzidis, M. G. Syntheses and characterization of the new homoleptic indium-polysulfide complexes [In2S27]4-, [In2S14]2-, and [In2S16]2. *Inorg. Chem.* **1993**, *32* (15), 3300−3305.
(84) Kaese, T.; Trageser, T.; Budy, H.; Bolte, M.; Lerner, H.-W.; Wagner, M. A redox-active diborane platform performs C(sp3)−H activation and nucleophilic substitution reactions. *Chem. Sci.* **2018**, *9* (15), 3881−3891.
(85) Trageser, T.; Bolte, M.; Lerner, H.-W.; Wagner, M. B−B Bond Nucleophilicity in a Tetraaryl μ-Hydridodiborane(4) Anion. *Angew. Chem., Int. Ed.* **2020**, *59* (20), 7726−7731.
(86) Cordero, B.; Gómez, V.; Platero-Prats, A. E.; Revés, M.; Echeverría, J.; Cremades, E.; Barragán, F.; Alvarez, S. Covalent radii revisited. *Dalton Trans.* **2008**, No. 21, 2832−2838.
(87) Hehre, W. J.; Ditchfield, R.; Pople, J. A. Self—Consistent Molecular Orbital Methods. XII. Further Extensions of Gaussian—Type Basis Sets for Use in Molecular Orbital Studies of Organic Molecules. *J. Chem. Phys.* **1972**, *56* (5), 2257−2261.
(88) Hariharan, P. C.; Pople, J. A. The influence of polarization functions on molecular orbital hydrogenation energies. *Theor. Chim. Acta* **1973**, *28* (3), 213−222.
(89) Ditchfield, R.; Hehre, W. J.; Pople, J. A. Self-Consistent Molecular-Orbital Methods. IX. An Extended Gaussian-Type Basis for Molecular-Orbital Studies of Organic Molecules. *J. Chem. Phys.* **1971**, *54* (2), 724−728.
(90) Dill, J. D.; Pople, J. A. Self-consistent molecular orbital methods. XV. Extended Gaussian-type basis sets for lithium, beryllium, and boron. *J. Chem. Phys.* **1975**, *62* (7), 2921−2923.
(91) Weigend, F.; Ahlrichs, R. Balanced basis sets of split valence, triple zeta valence and quadruple zeta valence quality for H to Rn: Design and assessment of accuracy. *Phys. Chem. Chem. Phys.* **2005**, *7* (18), 3297−3305.
(92) Peterson, K. A.; Figgen, D.; Goll, E.; Stoll, H.; Dolg, M. Systematically convergent basis sets with relativistic pseudopotentials. II. Small-core pseudopotentials and correlation consistent basis sets for the post-d group 16−18 elements. *J. Chem. Phys.* **2003**, *119* (21), 11113−11123.
(93) Lee, C.; Yang, W.; Parr, R. G. Development of the Colle-Salvetti correlation-energy formula into a functional of the electron density. *Phys. Rev. B* **1988**, *37* (2), 785−789.
(94) Becke, A. D. Density-functional thermochemistry. III. The role of exact exchange. *J. Chem. Phys.* **1993**, *98* (7), 5648−5652.
(95) Grimme, S.; Ehrlich, S.; Goerigk, L. Effect of the damping function in dispersion corrected density functional theory. *J. Comput. Chem.* **2011**, *32* (7), 1456−1465.
(96) Miertuš, S.; Scrocco, E.; Tomasi, J. Electrostatic interaction of a solute with a continuum. A direct utilizaion of AB initio molecular potentials for the prevision of solvent effects. *Chem. Phys.* **1981**, *55* (1), 117−129.
(97) Marenich, A. V.; Cramer, C. J.; Truhlar, D. G. Universal Solvation Model Based on Solute Electron Density and on a Continuum Model of the Solvent Defined by the Bulk Dielectric Constant and Atomic Surface Tensions. *J. Phys. Chem. B* **2009**, *113* (18), 6378−6396.
(98) Kabsch, W. A solution for the best rotation to relate two sets of vectors. *Acta Crystallogr., Sect. A* **1976**, *32* (5), 922−923.
(99) Kromann, J. C.; Bratholm, L. A. *Calculate Root-Mean-Square Deviation (RMSD) of Two Molecules Using Rotation*, GitHub 2019. http://github.com/charnley/rmsd.
(100) McClure, D. S. Triplet-Singlet Transitions in Organic Molecules. Lifetime Measurements of the Triplet State. *J. Chem. Phys.* **1949**, *17* (10), 905−913.
(101) Kasha, M. Collisional Perturbation of Spin-Orbital Coupling and the Mechanism of Fluorescence Quenching. A Visual Demonstration of the Perturbation. *J. Chem. Phys.* **1952**, *20* (1), 71−74.

(102) McGlynn, S. P.; Sunseri, R.; Christodouleas, N. External Heavy-Atom Spin-Orbital Coupling Effect. I. The Nature of the Interaction. *J. Chem. Phys.* **1962**, *37* (8), 1818−1824.
(103) Tokoro, Y.; Nagai, A.; Kokado, K.; Chujo, Y. Synthesis of Organoboron Quinoline-8-thiolate and Quinoline-8-selenolate Complexes and Their Incorporation into the π-Conjugated Polymer Main-Chain. *Macromolecules* **2009**, *42* (8), 2988−2993.
(104) Harris, R. K.; Becker, E. D.; Menezes, S. M. C. d.; Goodfellow, R.; Granger, P. NMR nomenclature. Nuclear spin properties and conventions for chemical shifts(IUPAC Recommendations 2001). *Pure Appl. Chem.* **2001**, *73* (11), 1795−1818.
(105) Frisch, M. J.; Trucks, G. W.; Schlegel, H. B.et al. *Gaussian 16 Rev. C.01*; Gaussian, Inc.: Wallingford, CT, 2016.
(106) Marques, M. A. L.; Gross, E. K. U. TIME-DEPENDENT DENSITY FUNCTIONAL THEORY. *Annu. Rev. Phys. Chem.* **2004**, *55* (1), 427−455.
(107) Yanai, T.; Tew, D. P.; Handy, N. C. A new hybrid exchange−correlation functional using the Coulomb-attenuating method (CAM-B3LYP). *Chem. Phys. Lett.* **2004**, *393* (1), 51−57.
(108) O'boyle, N. M.; Tenderholt, A. L.; Langner, K. M. cclib: A library for package-independent computational chemistry algorithms. *J. Comput. Chem.* **2008**, *29* (5), 839−845.
(109) Goddard, T. D.; Huang, C. C.; Meng, E. C.; Pettersen, E. F.; Couch, G. S.; Morris, J. H.; Ferrin, T. E. UCSF ChimeraX: Meeting modern challenges in visualization and analysis. *Protein Sci.* **2018**, *27* (1), 14−25.
(110) Pettersen, E. F.; Goddard, T. D.; Huang, C. C.; Meng, E. C.; Couch, G. S.; Croll, T. I.; Morris, J. H.; Ferrin, T. E. UCSF ChimeraX: Structure visualization for researchers, educators, and developers. *Protein Sci.* **2021**, *30* (1), 70−82.
(111) Meng, E. C.; Goddard, T. D.; Pettersen, E. F.; Couch, G. S.; Pearson, Z. J.; Morris, J. H.; Ferrin, T. E. UCSF ChimeraX: Tools for structure building and analysis. *Protein Sci.* **2023**, *32* (11), No. e4792.
(112) Neese, F. Software update: The ORCA program system—Version 5.0. *WIREs Comput. Mol. Sci.e* **2022**, *12* (5), No. e1606.
(113) Knizia, G. Intrinsic Atomic Orbitals: An Unbiased Bridge between Quantum Theory and Chemical Concepts. *J. Chem. Theory Comput.* **2013**, *9* (11), 4834−4843.
(114) Lu, T.; Chen, F. Multiwfn: A multifunctional wavefunction analyzer. *J. Comput. Chem.* **2012**, *33* (5), 580−592.
(115) Jimp 2. http://www.chem.tamu.edu/jimp2/index.html.

https://doi.org/10.1021/acs.inorgchem.4c02459
Inorg. Chem. 2024, 63, 17639−17650